Applied Clay Science 261 (2024) 107590

Contents lists available at ScienceDirect

Applied Clay Science

journal homepage: www.elsevier.com/locate/clay

Research Paper

Synthesis of NiCuMgAl-layered double hydroxides using advanced microwave and ultrasound methods

Judith Granados-Reyes, Angie C. Rueda, Yolanda Cesteros *

Universitat Rovira i Vigili, Departament de Química Física i Inorgànica, C/Marcel·lí Domingo, 1, 43007 Tarragona, Spain

ARTICLE INFO

Keywords:
Layered double hydroxides
Microwaves
Ultrasound
Autoclave
Basicity properties
Surface properties

ABSTRACT

The effect of using ultrasound vs magnetic stirring, microwaves vs conventional heating, and autoclave vs refluxing on the synthesis of NiCuMgAl-layered double hydroxides (LDH) was widely studied. The use of ultrasounds during coprecipitation resulted in lower LDH crystallinity, difficulted the incorporation of the divalent cations in the layer and led to low specific surface area and low basicity. This could be attributed to smaller crystallization nuclei formed under ultrasound; that is, more efficient agitation due to cavitation phenomena, led to less crystal growth. The use of microwaves refluxing during the aging step instead of conventional heating resulted in higher crystallinity, allowing a better incorporation of the cations in the layer, obtaining higher specific surface area and higher amount of stronger basic sites. Interestingly, the use of autoclave at higher temperature (180 °C) but at shorter time (1 h) improved the crystallinity of the LDH samples, especially in the stacking direction and applying microwaves, favoring the incorporation of the cations in the layer. Autoclave under microwaves led to higher amount of basic sites but lower surface area than autoclave by conventional heating at the same conditions. This suggests that microwaves favored a better incorporation of the hydroxyl groups into the layers and/or the appearance of surface-defective sites.

1. Introduction

Hydrotalcite-like materials, also called Layered Double Hydroxides (LDH), are inorganic compounds, with general formula $[M(II)_{1-x}M(III)_x(OH)_2]^{x+}[A^{n-}]_{x/n}{\cdot}mH_2O$, valued for their versatility, affordability and non-toxicity. The partial substitution of M(II) by M(III), which are divalent and trivalent cations (e.g., Mg^{2+} and Al^{3+}, respectively), generates a positive charge of the layers balanced by the presence of anions A^{n-} in the interlayer space. The specific composition of the LDH may vary based on the synthesis conditions and the metallic cations used, which influence the physicochemical properties of the material. Thus, hydrotalcites have been widely adapted for different applications such as catalysis, adsorption, gas storage/release, controlled drug release, and environmental remediation (Kostić et al., 2018; Lopes et al., 2018; Naseem et al., 2019).

The incorporation of Ni^{2+} or Cu^{2+} cations into hydrotalcites results, after calcination-reduction, in effective supported bimetallic NiCu heterogeneous catalysts for different reactions of interest, such as hydrogenation (Gupta and Kantam, 2018; Luo et al., 2021; Wu et al., 2017) fuel synthesis (Li et al., 2022; Wang et al., 2022; Wei et al., 2022, 2023), and energy conversion reactions (An et al., 2021; Lee et al., 2022; Summa et al., 2022; Yu et al., 2016).

NiCuMgAl-LDH have been prepared using different methods, such as urea coprecipitation (Wei et al., 2022, 2023) or metal ion adsorption (Wang et al., 2022); however, the most commonly approach involves traditional coprecipitation of the precursor salts under magnetic stirring followed by a long-time aging step using conventional refluxing heating. Yu et al. (2016) prepared NiCuMgAl hydrotalcites by coprecipitating the nitrate salts at 60 °C with NaOH at constant pH 10 and subsequent conventional aging at 60 °C for 19 h. Wu et al. (2017) synthesized coprecipitated at pH 9–10 CuNiMgAl-LDH with different Cu/Ni ratios, followed by a 20 h conventional aging at 80 °C. Gupta and Kantam (2018) synthesized a CuNiMgAl-LDH by coprecipitation at pH 9–10 subjected to an aging step of 4 h at room temperature followed by 4 h at 70 °C. The resulting material exhibited high crystallinity and a uniform distribution of cations within the brucite-like layers. Wang et al. (2018) synthesized several NiCuMgAl-LDH, with $Ni^{2+}/(Cu^{2+} + Ni^{2+})$ ratios from 0 to 0.4, by coprecipitation at 60 °C at pH 10 and aging at 60 °C for 6 h. The study concluded that introducing Ni reduced the sheet thickness of the hydrotalcite-type structure, improving the dispersibility of CuO

* Corresponding author at: Dpt. Química Física i Inorgànica, Universitat Rovira i Virgili, C/Marcel·lí Domingo 1, 43007 Tarragona, Spain.
E-mail address: yolanda.cesteros@urv.cat (Y. Cesteros).

https://doi.org/10.1016/j.clay.2024.107590
Received 19 May 2024; Received in revised form 1 October 2024; Accepted 2 October 2024
Available online 13 October 2024

particles and creating strongly basic sites. More recently, Summa et al. (2022) prepared NiCuMgAl hydrotalcite-like materials containing 15 wt % of nickel by coprecipitation at 65 °C with pH 9.5–10 and conventional aging at 65 °C for 1 h. Lee et al. (2022) synthesized several NiCuMgAl-LDH at pH 10 using conventional aging step at 60 °C for 16 h. On the whole, all samples exhibited the hydrotalcite phase although those with higher Cu/Ni molar ratios showed, additionally, the presence of CuO.

New synthesis methodologies, particularly microwave and ultrasound-assisted technologies, provided important advantages like uniform temperature distribution, rapid mass transfer, and the potential for finer particle sizes and shorter synthesis temperatures/times (Bergadà et al., 2007; Benito et al., 2007; Benito et al., 2008; Coral et al., 2019; Cosano et al., 2020; Fan et al., 2020; Granados-Reyes et al., 2014; Houssaini et al., 2021; Trujillano et al., 2018).

Diverse hydrotalcite-like compounds containing Ni or Cu were synthesized using microwaves (Álvarez et al., 2013; Ayala et al., 2011; Bergadà et al., 2007; Co-Al Ni-Al Viky-C Mujica-F et al., 2015; Gao et al., 2023; Niu et al., 2022; L. Wang et al., 2010). Nevertheless, to our knowledge, there are not studies on the preparation of NiCuMgAl-LDH using microwaves for the aging step or applying ultrasounds during coprecipitation, or using autoclave instead of traditional refluxing. Additionally, there is a lack of information in the characterization of the physicochemical properties of the NiCuMgAl-LDH conventionally prepared since more focus has been placed on the characterization of the calcined and reduced forms for catalytic applications.

The aim of this work is to investigate the impact of using microwave and ultrasound technologies for the synthesis of NiCuMgAl-LDH. These materials will be prepared using the coprecipitation method of the precursor salts at constant pH applying ultrasounds or magnetic stirring, while the aging step will be made with microwaves by autoclaving or refluxing. Special attention will be paid to the study of the surface and basic properties of the synthesized materials compared with those of LDH samples prepared by conventional heating.

2. Experimental

2.1. Samples preparation

Several NiCuMgAl hydrotalcite-like materials, with M^{2+}/M^{3+} molar ratio = 3, Mg^{2+}/Al^{3+} molar ratio = 1:1, and variable Ni^{2+}/Cu^{2+} molar ratio, were prepared by co-precipitation of the corresponding salts at 80 °C and subsequent aging. Some of the coprecipitation conditions used, such as the type of salts, concentration, precipitation and aging temperature, were the same than those used by Wu et al. (2017) for synthesizing NiCuMgAl-LDHs by conventional refluxing. However, to study the effect of using ultrasound vs magnetic stirring, microwaves vs conventional heating, and autoclave vs refluxing on the synthesis, different methodologies were applied during coprecipitation and in the aging stages, leading to different LDH materials (Table 1).

A first series of samples were prepared with Ni^{2+}/Cu^{2+} molar ratio of 1. In a typical synthesis, 0.4 mol L^{-1} aqueous solution containing the appropriate amounts of $Ni(NO_3)_2{\cdot}6H_2O$ (Sigma-Aldrich), $Cu(NO_3)_2{\cdot}3H_2O$ (Sigma-Aldrich), $Al(NO_3)_3{\cdot}9H_2O$ (Sigma-Aldrich), $Mg(NO_3)_2{\cdot}6H_2O$ (Sigma-Aldrich) was added dropwise to a 500 mL three neck round-bottom flask containing 200 mL of a 0.1 mol L^{-1} $Na_2CO_3{\cdot}10H_2O$ solution. The pH was kept constant at 9.5 ± 0.1 by the simultaneous addition of an aqueous solution 1.5 mol L^{-1} of NaOH (Panreac) under magnetic stirring and using a pHmeter. After complete addition of the metallic salts, the mother solutions were aged by different treatments: microwaves refluxing at 80 °C for 5 h (NiCuMw); microwaves autoclave at 180 °C for 1 h (NiCuMwA); conventional refluxing at 80 °C for 20 h (NiCuConv) or 5 h ($NiCuConv_5$), and conventional autoclave at 180 °C for 1 h (NiCuConvA). The microwaves equipment used was a Milestone FlexiWAVE laboratory apparatus working at frequency of 2.45 GHz and equipped with a controller temperature (ATC-400). The irradiation microwave was programmed to work at a maximum of 800 W. Two more samples were prepared by using an ultrasound bath (Selecta, sound wave frequency of 40 Hz, 150 W) during the coprecipitation of the precursor salts for 30 min instead of magnetic stirring. Then, samples were aged by microwaves autoclave at 180 °C for 1 h (NiCuUsMwA) and conventional refluxing at 80 °C for 20 h (NiCuUsConv).

In order to study the effect of the Ni^{2+}/Cu^{2+} molar ratio, other group of samples was prepared following the same coprecipitation method but with Ni^{2+}/Cu^{2+} molar ratio of 2 and 4 choosing some synthesis conditions. Samples were aged with microwaves refluxing at 80 °C for 5 h (Ni_2CuMw and Ni_4CuMw), and by conventional refluxing at 80 °C for 20 h ($Ni_2CuConv$ and $Ni_4CuConv$). Two more samples were prepared using ultrasound instead of magnetic stirring during coprecipitation ($Ni_2CuUsConv$ and $Ni_4CuUsConv$). After aging, samples were filtered and washed with deionized water until neutral pH, and dried at 80 °C for 24 h. The main preparation and aging conditions of the samples prepared are shown in Table 1.

2.2. X-ray diffraction (XRD)

The acquisition of powder X-ray diffraction (XRD) patterns was conducted using a Siemens D5000 diffractometer employing CuKα radiation filtered through nickel, possessing a wavelength (λ) of 1.45 Å. The CuKα radiation source was derived from an X-ray copper tube, operating at specific conditions of 40 kV and 30 mA. The data collection procedure involved capturing diffraction patterns within the angular range of 2θ values from 5° to 80°, employing an incremental angular step of 0.05°. Each data acquisition occurred over a period of 3 s in simple rotation. Crystalline phase was identified using the Joint Committee on Powder Diffraction Standard (JCPDS) file 089–0460-hydrotalcite. Cell parameters 'a' ($a = 2d_{110}$) and 'c' ($c = 3d_{003}$) were determined from 110 and 003 reflections, respectively. Individual peaks were fitted with the TOPAS v6 software (Coelho, 2018). The background was modelled with a 2nd order Chebyschev polynomial. The instrumental contribution to the diffraction profile was calculated with the

Table 1
Preparation conditions of the NiCuMgAl-LDH samples.

Sample	Ni/Cu molar ratio	Stirring during precipitation	Aging method	Aging temperature (°C)	Aging time (h)
NiCuConv	1:1	magnetic stirring	conventional refluxing	80	20
NiCuMw	1:1	magnetic stirring	microwave refluxing	80	5
$NiCuConv_5$	1:1	magnetic stirring	conventional refluxing	80	5
NiCuUsConv	1:1	ultrasound	conventional refluxing	80	20
NiCuConvA	1:1	magnetic stirring	conventional autoclave	180	1
NiCuMwA	1:1	magnetic stirring	microwave autoclave	180	1
NiCuUsMwA	1:1	ultrasound	microwave autoclave	180	1
$Ni_2CuConv$	2:1	magnetic stirring	conventional refluxing	80	20
Ni_2CuMw	2:1	magnetic stirring	microwave refluxing	80	5
$Ni_2CuUsConv$	2:1	ultrasound	conventional refluxing	80	20
$Ni_4CuConv$	4:1	magnetic stirring	conventional refluxing	80	20
Ni_4CuMw	4:1	magnetic stirring	microwave refluxing	80	5
$Ni_4CuUsConv$	4:1	ultrasound	conventional refluxing	80	20

LaB6 (NIST SRM 660c). The peak width was obtained by fitting a Lorentzian contribution of the crystallite size effect and discarding any contribution of the microstrain to the peak width. The integral breadth of each peak was obtained from the fitted Lorentziab function. The Scherrer equation (Stokes and Wilson, 1942) was then applied to obtain the apparent crystallite size.

2.3. Elemental analysis

Elemental analysis of the hydrotalcites were obtained with an Induced Coupled Plasma – Optical Emission Spectroscopy analyzer (ICP-OES) from Spectro Arcos. The digestion of all hydrotalcites was carried out with concentrated HNO_3. Analyses were performed by triplicate.

2.4. High-resolution transmission electron microscopy (HRTEM)

High-Resolution Transmission electron microscopy of the samples was performed using a JEOL F200 TEM ColdFEG equipment with an operating voltage of 200 kV. Samples were dispersed in ethanol and a drop of the suspension was poured on to a carbon coated cooper grip and dried at room temperature before measurements. HRTEM images were acquired with a Gatan OneView camera, a CMOS-based and optical fibre-coupled detector of 4096 by 4096 pixels. Gatan Digital Micrograph program was used to process the TEM images.

2.5. Thermogravimetric analysis (TGA)

Thermogravimetric analysis was carried out in a Mettler Toledo TGA 2 equipped with a 20–1100 °C programmable temperature furnace. The accuracy was ±1 μg. Approximately 40 mg of sample was heated in a N_2 flow (50 mL/min) from 25 to 800 °C at rate of 5 °C/min.

2.6. Nitrogen physisorption

BET specific surface areas were calculated from the nitrogen adsorption isotherms at −196 °C using a Micromeritic 3FLEX surface analyzer and a value of 0.164 nm^2 for the cross-section of the nitrogen molecule. Brunauer, Emmett and Teller (BET) theory was applied to calculate the total specific surface area of the samples and the Barrett, Joyner & Halenda (BJH) method was used to calculate the pore size distribution. Samples were degassed at 120 °C for 6 h prior to the analysis.

2.7. Acid titration

The basic sites density of the samples was determined by titration with 0.01 mol L^{-1} solution of benzoic acid in toluene using 0.05 g of the sample mixed and stirred for 30 min in 2 mL of indicator solution. For the determination of weak basic sites (pKa = 7.1) the indicator solution contained 0.1 mg/mL of bromothymol blue while for the determination of strong basic sites (pKa = 9.3), 0.1 mg/mL of phenolphthalein was used (Chang et al., 2019).

2.8. CO_2-temperature programmed desorption (CO_2-TPD)

To obtain more information about the basicity of this type of materials, the amount and strength of the basic centers of the NiCuMgAl-LDH samples were determined by CO_2-TPD technique. CO_2-TPD analysis were performed using Autochem III-Micromeritics, 100 mg of sample was pretreated at 120 °C with He flow (10 °C/min for 30 min), after that, the sample was saturated with pure CO_2 (80 °C for 10 min). CO_2 desorption was performed with He from 150 °C to 800 °C at 5 °C/min (all flow rates were set at 50 mL/min). In addition, a thermogram was recorded without CO_2 treatment, as blank.

3. Results and discussion

3.1. X-ray diffraction (XRD)

XRD patterns of the NiCuMgAl-LDH prepared with Ni^{2+}/Cu^{2+} molar ratio of 1 showed one crystalline phase due to the hydrotalcite phase (JCPDS 89–0460), regardless of the preparation method, with sharp and intense peaks corresponding to the 003, 006, 012 reflections, and broader and less intense peaks, for the 015, 018, 110 and 113 reflections (Fig. 1a). By increasing the Ni^{2+}/Cu^{2+} molar ratio, the hydrotalcite crystallinity increased showing a better definition of the peaks, especially at higher 2θ angles (Fig. 1b). This can be explained by the decrease of the Jahn-Teller effect of Cu^{2+}, which makes its incorporation into the brucite-like layers difficult (Yu et al., 2016).

The crystallite size values, calculated using the Scherrer equation for the 003 and 110 reflections corresponding to the stacking and lamella direction, respectively, and the cell parameters values, calculated from the XRD patterns are indicated in Table 2.

Regarding NiCuMgAl-LDH samples with Ni^{2+}/Cu^{2+} molar ratio of 1, the crystallite size values were higher both in the stacking and in the lamella direction for the samples aged using microwaves (NiCuMw and NiCuMwA) with respect to those aged at the same temperature and time by conventional heating ($NiCuConv_5$ and NiCuConvA, respectively) (Table 2).

This behavior was previously observed for other LDH (L. Wang et al., 2010), and can be attributed to the most homogeneous heating of microwaves (Álvarez et al., 2013). The increase of the aging time (NiCuConv vs. $NiCuConv_5$) increased the crystallinity of the hydrotalcite, as expected (Table 2).

The use of autoclave at higher temperature (180 °C) but at shorter time (1 h) improved the crystallinity of the LDH samples, especially in the stacking direction and using microwaves. Thus, NiCuMwA, aged with autoclave at 180 °C for 1 h under microwaves, had higher crystallite size values than the sample aged by refluxing at 80 °C for 5 h under microwaves (NiCuMw). This trend was previously reported for NiMgAl-LDHs (Bergadà et al., 2007) or ZnAl-LDHs (Benito et al., 2008) prepared under microwaves. This effect was minor for the samples prepared by conventional heating, in which NiCuConvA had slightly higher crystallite size values than $NiCuConv_5$ (Table 2). These results confirmed the positive effect of microwaves on the crystallinity of the samples. This can be explained by the Ostwald ripening growth mechanism, in which the small particles are dissolved and precipitate into the bigger ones to give larger and better crystallized materials (Benito et al., 2008). Thus, the fast enhancement under microwaves allows obtaining higher crystalline materials at shorter aging times.

Interestingly, the application of ultrasound during coprecipitation of the salts instead of magnetic stirring resulted in hydrotalcite-like materials with lower crystallite size values both using conventional heating (NiCuUsConv vs NiCuConv) and microwaves (NiCuUsMwA vs NiCuMwA). This could be related to the fact that the formed crystallization nuclei were smaller under ultrasounds, due to its more effective stirring, and consequently, during the aging step, they grew less. Cavitation, which involves the formation, growth, and implosive collapse of bubbles in a liquid, significantly enhances the mixing and mass transfer processes. This effect was less significant for the microwaved samples especially regarding the variation of the crystallite size values of the lamellae (Table 2).

By increasing the Ni^{2+}/Cu^{2+} molar ratio (2:1 and 4:1), on the whole, the crystallite size values increased (Table 2). This can be due to the better distribution of Cu^{2+} cations in the hydrotalcite lamella. As the Ni^{2+}/Cu^{2+} molar ratio increased, Cu^{2+} cations are more distant one from each other, diminishing their Jahn Teller effect, improving the octahedral structure of the lamella, and therefore, the hydrotalcite crystallinity increased (Yu et al., 2016). Again, the ultrasonic stirred samples ($Ni_2CuUsConv$ and $Ni_4CuUsConv$) were less crystalline than the corresponding samples prepared by magnetic stirring ($Ni_2CuConv$ and

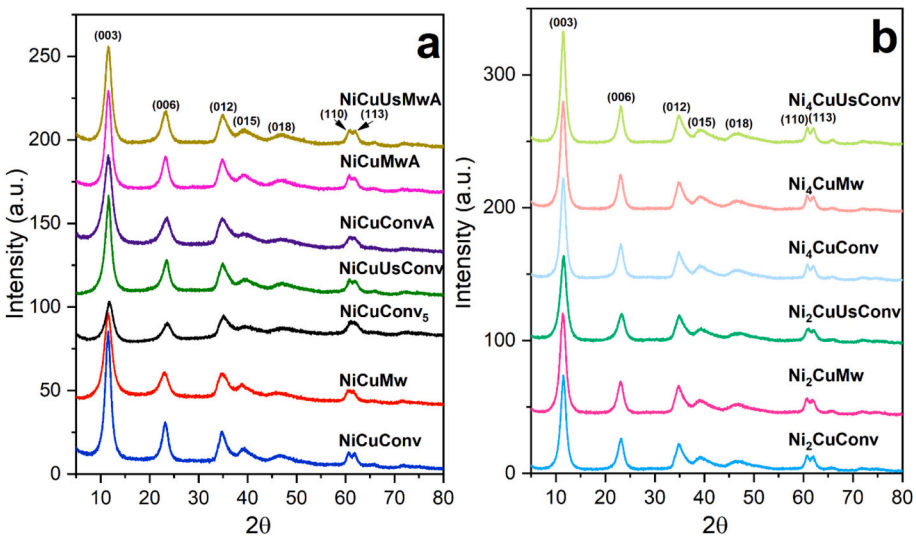

Fig. 1. XRD patterns of the synthesized a) NiCuMgAl-LDH samples with Ni^{2+}/Cu^{2+} molar ratio = 1; and b) NiCuMgAl-LDH samples with Ni^{2+}/Cu^{2+} molar ratio = 2 and 4.

Table 2
Characterization of the synthesized NiCuMgAl-hydrotalcite-like materials.

Sample	Experimental formula	Crystallite size (nm) 003 [a]	Crystallite size (nm) 110 [a]	Lattice parameters (Å) [a]		Molar ratio [b]				
				c	*a*	Ni^{2+}/Cu^{2+}	Ni^{2+}/Al^{3+}	Cu^{2+}/Al^{3+}	Mg^{2+}/Al^{3+} (1.00)	M^{2+}/M^{3+} (3.00)
NiCuConv	$[Ni_{0.25}Cu_{0.27}Mg_{0.24}Al_{0.24}(OH)_2]$ $[(CO_3^{2-})_{0.08}(NO_3^-)_{0.08}]\cdot 0.37H_2O$	4.1	7.9	23.0	3.05	0.89 (1.00)	1.00	1.11	1.00	3.11
NiCuMw	$[Ni_{0.25}Cu_{0.26}Mg_{0.25}Al_{0.24}(OH)_2]$ $[(CO_3^{2-})_{0.08}(NO_3^-)_{0.08}]\cdot 0.32H_2O$	3.4	7.3	22.9	3.06	0.92 (1.00)	1.03	1.05	1.01	3.09
$NiCuConv_5$	$[Ni_{0.24}Cu_{0.25}Mg_{0.24}Al_{0.27}(OH)_2]$ $[(CO_3^{2-})_{0.08}(NO_3^-)_{0.11}]\cdot 0.27H_2O$	2.7	5.3	23.0	3.05	0.96 (1.00)	1.26	1.32	0.91	2.72
NiCuUsConv	$[Ni_{0.27}Cu_{0.31}Mg_{0.14}Al_{0.28}(OH)_2]$ $[(CO_3^{2-})_{0.08}(NO_3^-)_{0.12}]\cdot 0.35H_2O$	3.7	5.6	22.9	3.05	0.89 (1.00)	1.00	1.12	0.51	2.63
NiCuConvA	$[Ni_{0.25}Cu_{0.27}Mg_{0.24}Al_{0.24}(OH)_2]$ $[(CO_3^{2-})_{0.06}(NO_3^-)_{0.12}]\cdot 0.38H_2O$	2.9	5.4	22.5	3.04	0.93 (1.00)	1.04	1.12	1.04	3.16
NiCuMwA	$[Ni_{0.25}Cu_{0.27}Mg_{0.24}Al_{0.24}(OH)_2]$ $[(CO_3^{2-})_{0.07}(NO_3^-)_{0.10}]\cdot 0.34H_2O$	4.0	7.5	22.9	3.05	0.92 (1.00)	1.03	1.12	0.97	3.11
NiCuUsMwA	$[Ni_{0.25}Cu_{0.24}Mg_{0.25}Al_{0.26}(OH)_2]$ $[(CO_3^{2-})_{0.07}(NO_3^-)_{0.12}]\cdot 0.28H_2O$	3.6	6.1	22.9	3.05	1.04 (1.00)	0.96	0.92	0.96	2.85
$Ni_2CuConv$	$[Ni_{0.34}Cu_{0.17}Mg_{0.24}Al_{0.24}(OH)_2]$ $[(CO_3^{2-})_{0.07}(NO_3^-)_{0.08}]\cdot 0.26H_2O$	4.5	8.2	23.0	3.05	1.95 (2.00)	1.39	0.71	0.99	3.10
Ni_2CuMw	$[Ni_{0.34}Cu_{0.17}Mg_{0.25}Al_{0.24}(OH)_2]$ $[(CO_3^{2-})_{0.08}(NO_3^-)_{0.08}]\cdot 0.28H_2O$	4.2	7.9	23.2	3.05	1.93 (2.00)	1.40	0.72	1.03	3.14
$Ni_2CuUsConv$	$[Ni_{0.35}Cu_{0.18}Mg_{0.21}Al_{0.26}(OH)_2]$ $[(CO_3^{2-})_{0.08}(NO_3^-)_{0.10}]\cdot 0.32H_2O$	3.7	6.6	23.0	3.04	1.88 (2.00)	1.37	0.76	0.79	2.87
$Ni_4CuConv$	$[Ni_{0.41}Cu_{0.10}Mg_{0.25}Al_{0.24}(OH)_2]$ $[(CO_3^{2-})_{0.08}(NO_3^-)_{0.08}]\cdot 0.36H_2O$	4.8	9.4	23.1	3.05	4.12 (4.00)	1.69	0.41	1.00	3.11
Ni_4CuMw	$[Ni_{0.41}Cu_{0.10}Mg_{0.23}Al_{0.24}(OH)_2]$ $[(CO_3^{2-})_{0.08}(NO_3^-)_{0.04}]\cdot 0.37H_2O$	4.5	9.0	23.1	3.05	4.00 (4.00)	1.69	0.42	0.98	3.09
$Ni_4CuUsConv$	$[Ni_{0.40}Cu_{0.10}Mg_{0.26}Al_{0.24}(OH)_2]$ $[(CO_3^{2-})_{0.08}(NO_3^-)_{0.08}]\cdot 0.41H_2O$	4.8	8.7	23.1	3.05	3.99 (4.00)	1.63	0.41	1.01	3.05

[a] Calculated from XRD results; [b] Determined from ICP results. The values between parentheses correspond to the theoretical molar ratio values.

$Ni_4CuConv$, respectively) (Table 2), confirming the negative effect of ultrasound on the crystallinity of the samples.

Cell parameters *a* and *c*, determined from the 110 and 003 reflections, respectively, were calculated to obtain information about the distribution of cations in the lamellae and in their stacking for all the hydrotalcites (Table 2). The cell parameter c is related to the electrostatic forces between the cations of the layers and the anions of the interlamellar space. The values obtained for the cell parameter *c* were similar in the range of 22.5 Å to 23.1 Å. The small variations could be related to the different distribution of the species in the interlamellar space, and lower c values suggest higher electrostatic interactions.

The cell parameter *a* indicates the average distance between the cations in the lamellae, which depends on the chemical composition. The values of the parameter *a* were practically constant in the whole group of hydrotalcites synthesized (3.05 Å), in agreement with the expected values since the ionic radio of the Ni^{2+} (0.72 Å) and Cu^{2+} (0.69 Å) cations are similar to the ionic radius of the Mg^{2+} (0.65 Å).

3.2. Elemental analysis

Elemental analysis was carried out by ICP to determine the chemical formulae of the hydrotalcites and investigate the possible variations of the cations content by the action of microwave or ultrasound technologies. The carbonate content was calculated from decomposition studies using a calibrated detector whereas the amount of nitrates was calculated as the difference between the total anions content, determined from the M^{2+}/M^{3+} molar ratio. The interlayer water was determined from TGA curves. The results are shown in Table 2.

The analysis of the M^{2+}/M^{3+} molar ratio of the hydrotalcites prepared with Ni^{2+}/Cu^{2+} molar ratio of 1 led to interesting differences between the samples. By comparing the hydrotalcites aged by refluxing, the sample aged with microwaves (NiCuMw) adjusted more to the theoretical M^{2+}/M^{3+} molar ratio (3.09), confirming a better incorporation of the cations in the layer, than the sample aged by conventional heating at the same temperature and time $NiCuConv_5$ (2.72) (Table 2). Much longer aging time under conventional heating (NiCuConv) were needed to reach the theoretical value (Table 2). These differences between microwaves and conventional heating were not observed when comparing the samples aged in autoclave (NiCuMwA and NiCuConvA) in which the M^{2+}/M^{3+} molar ratio values were similar for both samples and around 3. Thus, the use of autoclave at higher temperature and time, favored the incorporation of the cations during the formation of the layers. It is important to emphasize that there are not previous results in the literature concerning the incorporation of more than two divalent cations in the hydrotalcite structure.

On the other hand, the use of ultrasound during coprecipitation both by conventional refluxing (NiCuUsConv) or by autoclave under microwaves (NiCuUsMwA) led to lower M^{2+}/M^{3+} molar ratio (2.62 and 2.85, respectively) when comparing with the corresponding samples prepared without ultrasound (3.11 for NiCuConv and 3.09 for NiCuMwA). This could indicate that the very efficient stirring of ultrasound difficulted the incorporation of the divalent cations in the layer. In the case of NiCuUsConv this can be explained mainly because Mg^{2+} was not incorporated properly in the layer ($Mg^{2+}/Al^{3+} = 0.51$) while for the NiCuUsMwA the lower incorporation of the different divalent cations was similar ($Ni^{2+}/Al^{3+} = 0.96$, $Cu^{2+}/Al^{3+} = 0.92$ and $Mg^{2+}/Al^{3+} =$

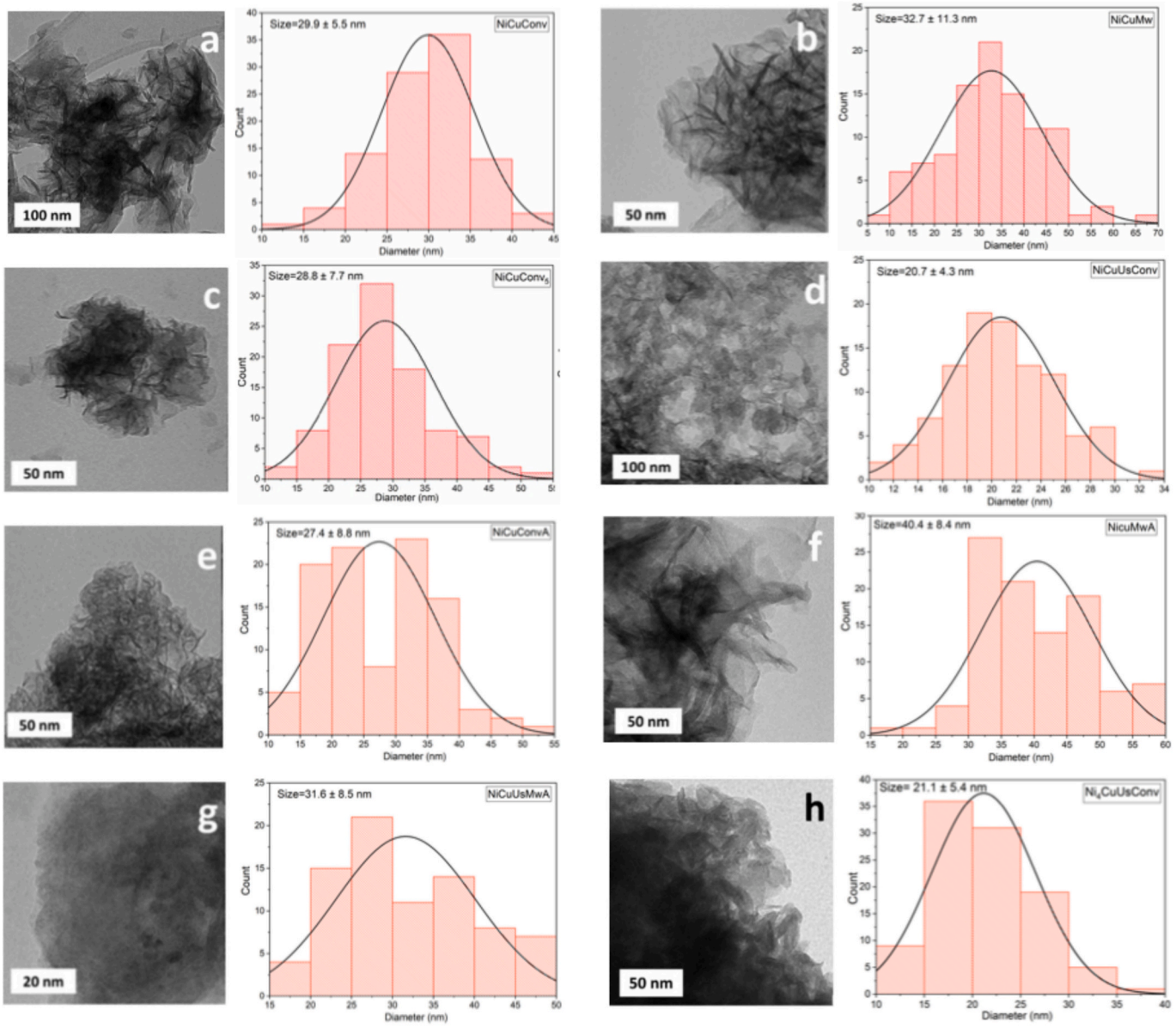

Fig. 2. HRTEM images and particles size distribution of (a) NiCuConv (150,000×), (b) NiCuMw (300,000×), (c) $NiCuConv_5$ (200,000×), (d) NiCuUsConv (120,000×), (e) NiCuConvA (200,000×), (f) NiCuMwA (300,000×), (g) NiCuUsMwA (500,000×), (h) $Ni_4CuUsConv$ (500,000×).

0.96). This different behavior could confirm the effect of autoclave, which seems to favor a better incorporation of the cations in the structure, as observed for the other autoclaved samples.

By increasing the Ni^{2+}/Cu^{2+} molar ratio up to 2 and 4, the M^{2+}/M^{3+} ratio was better adjusted to the expected theoretical value for all samples (Table 2), even for those stirred under ultrasounds. This means that by decreasing the amount of copper in the structure, there was a better arrangement of the divalent cations in the layer, as reported in previous studies. Anyway, again the M^{2+}/M^{3+} ratio values for the samples stirred with ultrasounds (Ni_2CuUsConv and Ni_4CuUsConv) were slightly lower than for the corresponding samples precipitated by magnetic stirring (Ni_2CuConv and Ni_4CuConv, respectively), especially for the sample with Ni^{2+}/Cu^{2+} molar ratio of 2. This confirms that the lower the amount of Cu^{2+} in the structure, the higher incorporation of Mg^{2+} since the Mg^{2+}/Al^{3+} molar ratio values increased in the order NiCuUsConv, Ni_2CuUsConv and Ni_4CuUsConv (Table 2). Therefore, the negative effect of ultrasounds on the incorporation of the divalent cations can be overcome using lower Cu^{2+} content.

3.3. High-resolution transmission electron microscopy (HRTEM)

HRTEM images of the NiCuMgAl-LDH samples showed the formation of the well-formed characteristic thin lamellae corresponding to the hydrotalcite-type materials (Fig. 2). No significant differences were observed in the micrographies between samples but, on the whole, the samples aged with microwaves showed higher lamellae sizes (e.g., Fig. 2b and f). This agrees with their higher crystallinity (Fig. 1). Interestingly, the samples precipitated under ultrasounds presented more ordered layers parallel to the grating surface (e.g., Fig. 2d, g and h), with lower particle sizes for the samples with Ni^{2+}/Cu^{2+} molar ratio of 1 due to their lower crystallinity (Fig. 1a).

The layers had average particle sizes between 20 and 40 nm. The particle size distribution of the samples was more homogeneous for the samples prepared by refluxing. This could be related to the higher aging time employed to prepare these samples. The average particle size (indicated on Fig. 2) was higher for the samples prepared under microwaves both by refluxing and by autoclave confirming the higher crystallinity of these samples, as observed by XRD.

By increasing the Ni^{2+}/Cu^{2+} molar ratio, the samples showed higher layer sizes (e.g., Fig. 2h) according to their higher crystallinity, as confirmed by XRD. The interlayer distances, calculated from the HRTEM micrographies, were slightly higher for the samples aged under microwaves (6.6–7 Å) than for those aged by conventional heating (4.9–6.2 Å). For the samples precipitated with ultrasounds, the interlayer distances were the highest, 6.2 Å for NiCuUsConv and 7 Å for NiCuUsMwA indicating less strength of interaction between the layers.

3.4. Thermogravimetric analysis (TGA)

TGA curves of the NiCuMgAl-LDH samples mainly showed two mass losses and, regarding the TGA profiles, the samples could be classified into two groups. The first group includes NiCuConv, $NiCuConv_5$, NiCuMw, NiCuConvA and NiCuMwA samples, and the second group corresponds to the NiCuUsMwA, NiCuUsConv, Ni_2CuConv, Ni_2CuMw, Ni_2CuUsConv, Ni_4CuConv, Ni_4CuMw and Ni_4CuUsConv samples. Two representative TGA curves of the two groups of samples are shown in Fig. 3 and the temperature maxima and the mass loss percentages for all of them are depicted in Table 4. For the samples of the first group, the two peaks had similar derivatives (e.g., Fig. 3a) while for the samples of the second group, the derivative of the second peak was more intense than that of the first peak (e.g., Fig. 3b, Table 3). The total mass loss was in the range 35.7–38.6 % for all samples (Table 3).

The first mass loss occurred between 100 °C and 240 °C, with mass losses percentages between 9 % and 15 %, and was due to physisorbed water and water located in the interlayer space. The temperature maxima of this first mass loss were lower for the samples with Ni^{2+}/Cu^{2+} molar ratio of 1 and increased as the molar ratio increased. Additionally, the mass loss was slower for the samples prepared with the Ni^{2+}/Cu^{2+} molar ratio of 2 and 4 (lower intensity of the derivative) (e.g., Fig. 3b). The second mass loss, which was observed in the temperature range of 280 °C to 500 °C with mass losses between 17 % and 26 %, was due to the dehydroxylation of the lamellae together with the loss of anions from the interlamellar space. Again, the temperature maxima were higher for the samples with higher Ni^{2+}/Cu^{2+} molar ratio (Table 3) and the range of temperature variation for this second mass loss was lower for these

Table 3
Data obtained from the thermogravimetric analysis of the NiCuMgAl-LDH samples.

Sample	First mass loss		Second mass loss		Total mass loss (%)
	T (°C)	wt (%)	T (°C)	wt (%)	
NiCuConv	177.0	13.9	360.0	18.2	38.5
NiCuMw	175.9	11.7	329.8	19.6	37.3
$NiCuConv_5$	175.0	14.0	320.5	17.4	36.8
NiCuUsConv	177.5	12.2	362.5	21.5	38.2
NiCuConvA	174.0	12.8	333.3	19.8	36.9
NiCuMwA	181.3	12.8	371.2	19.4	38.3
NiCuUsMwA	190.0	10.3	383.5	21.2	35.7
Ni_2CuConv	192.7	8.7	389.5	25.5	38.2
Ni_2CuMw	190.8	10.2	378.0	24.7	38.9
Ni_2CuUsConv	203.7	11.7	369.8	21.6	38.5
Ni_4CuConv	198.0	11.3	391.0	23.3	38.4
Ni_4CuMw	208.0	13.4	381.5	21.4	38.5
Ni_4CuUsConv	217.7	15.1	380.3	19.5	38.6

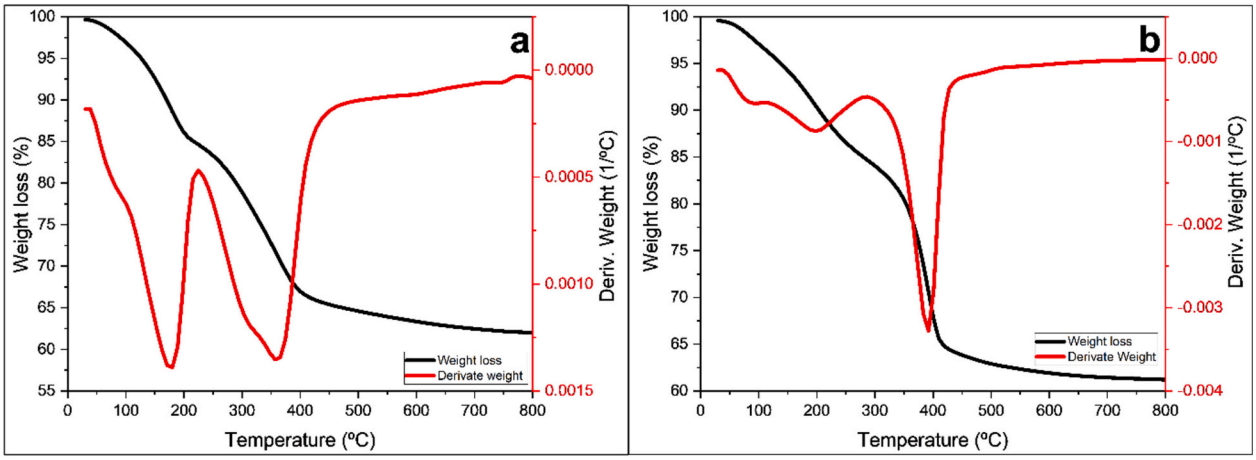

Fig. 3. TGA curves of (a) NiCuConv, (b) Ni_4CuConv.

samples (e.g., Fig. 3b). This can be explained by the higher crystallinity and better incorporation of the Cu^{2+}, and therefore, better construction of the layers, observed for the samples with higher Ni^{2+}/Cu^{2+} molar ratio (Table 2).

Regarding the effect of microwaves for the samples prepared at the same temperature and time by refluxing (NiCuMw vs $NiCuConv_5$) or autoclaving (NiCuConvA vs NiCuMwA), slight higher temperature maxima were observed for the microwaved samples in both cases (Table 3). This can be related to their higher crystallinity (Table 1).

Interestingly, the use of ultrasounds for the Ni^{2+}/Cu^{2+} samples with molar ratio of 1 led to higher temperature maxima and slower mass loss for the first mass loss although these samples were less crystalline (Table 2). This could be related to a higher stacking of the layers, as observed by HRTEM (Fig. 2). For the samples prepared with ultrasounds at higher molar ratio (Ni_2CuUsConv and Ni_4CuUsConv), the temperature maxima of the first mass loss and the second mass loss were higher than those of the sample with lower Ni^{2+}/Cu^{2+} ratio NiCuUsConv (Table 3). This could be explained by the higher crystallinity observed for the samples prepared at higher Ni^{2+}/Cu^{2+} ratio with a better construction of the hydrotalcite structure.

Finally, the base line never became linear, suggesting further decomposition of the sample with an average loss of 0.8 % of the total mass percentage lost. This loss may be due to the removal of strongly retained carbonate species (Álvarez et al., 2013).

3.5. Study of the surface and basic properties of several NiCuMgAl-LDH samples

In order to study the effect of microwaves vs conventional heating, autoclave vs refluxing and ultrasounds vs magnetic stirring on the surface and basic properties of the NiCuMgAl-LDH, nitrogen physisorption, benzoic acid titration and CO_2-TPD of the samples of Ni^{2+}/Cu^{2+} ratio of 1: NiCuConv, NiCuMw, $NiCuConv_5$, NiCuUsConv, NiCuConvA, NiCuMwA and NiCuUsMwA, were carried out.

3.5.1. Surface properties

The main nitrogen physisorption characterization results are shown

Table 4
Surface and basic properties of the NiCuMgAl hydrotalcite-like samples.

Sample	Specific surface area (m^2/g)	Benzoic acid titration		CO_2-TPD (mmol CO_2/g)
		Weak basic sites (mmol/g)	Strong basic sites (mmol/g)	
NiCuConv	72	0.05	0.30	0.14
NiCuMw	148	–	0.34	0.26
$NiCuConv_5$	44	–	0.08	0.02
NiCuUsConv	6	0.02	0.06	0.11
NiCuConvA	120	–	0.16	0.11
NiCuMwA	32	0.06	0.32	0.29
NiCuUsMwA	10	0.02	0.14	0.05

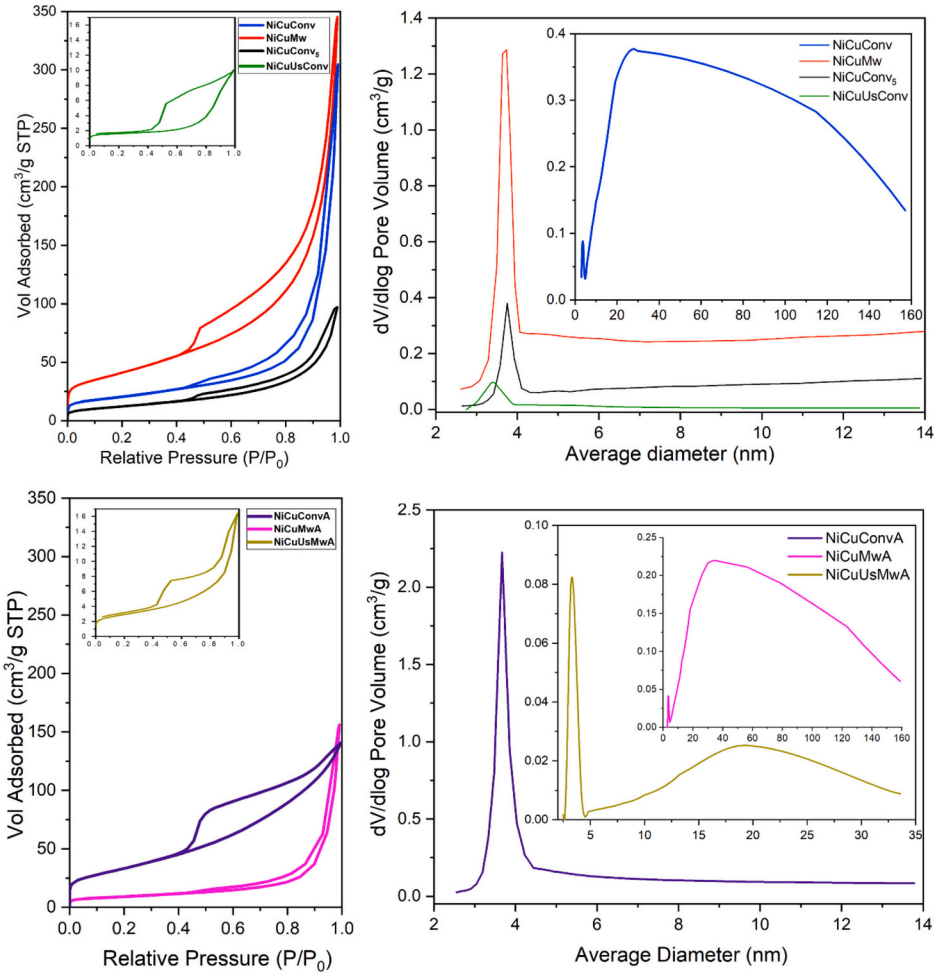

Fig. 4. N_2 adsorption-desorption isotherms (left) and BJH pore size distribution graphics in the desorption way (right) of the NiCuMgAl-LDH samples with Ni/Cu molar ratio of 1.

in Fig. 4 and Table 4. All NiCuMgAl-LDH samples exhibited nitrogen adsorption-desorption isotherms of type IV, according to the IUPAC classification, which are characteristic of isotherms with hysteresis at high pressures and mesoporous character. It is important to remark, that the use of ultrasounds during coprecipitation (NiCuUsConv, NiCuUsMwA) led to a significant decrease in the nitrogen adsorption (Fig. 4), and consequently, these samples had the lowest specific surface area values (Table 4). This could be attributed to the intercalated anions avoiding nitrogen penetration as observed for other hydrotalcites of low specific surface area (Ayala et al., 2011).

All hydrotalcite-like materials showed type H3 hysteresis loop, according to the IUPAC classification, characteristic of disordered distribution of lamellae, between which there are empty spaces, forming slit-like pores. For the samples NiCuMw, NiCuConvA, NiCuUsConv, and NiCuUsMwA a widening of the hysteresis, which was more marked for the samples coprecipitated under ultrasounds, was observed (NiCuUsConv and NiCuUsMwA in Fig. 4). This could be related to the presence of mesopores with lower sizes, as observed in the corresponding pore size distribution graphics (Fig. 4), and to a higher stacking of layers, as observed by HRTEM for the samples precipitated with ultrasounds (Fig. 2d and g).

Pore size distribution graphic of the sample NiCuConv, aged by conventional refluxing, showed a main and wide peak with maximum around 40 nm (Fig. 4), which agreed with the typical porosity described for the hydrotalcites obtained by conventional refluxing at longer times (Bergadà et al., 2007; Cavani et al., 1991). However, for the samples $NiCuConv_5$ and NiCuMw, aged at the same temperature but at shorter time (5 h), the main peak was observed with maximum around 4 nm, with much higher nitrogen adsorbed volume for the microwaved sample, resulting in much higher specific surface area for this sample (Table 4). Therefore, microwaves favored the formation of high amounts of low-size mesoporous under refluxing conditions. This could be related to some disaggregation of the hydrotalcite layers during microwave treatment although we cannot completely discard the presence of small amounts of insoluble amorphous species.

Interestingly, for the autoclaved samples, the behavior was the opposite. Thus, the sample aged in autoclave under microwaves (NiCuMwA) showed a main peak with maximum at higher mesopore size (40 nm) than the corresponding sample aged by conventional heating at the same temperature and time (NiCuConvA), which had a main peak with maximum at around 4 nm (Fig. 4) and higher specific surface area (Table 4). This means that the use of autoclave under microwaves at these conditions was so efficient in the development of the hydrotalcite-like structure than the traditional hydrotalcites aged under conventional refluxing at longer time achieving similar pore size distribution at shorter time (1 h).

Finally, the pore size distribution graphics for the samples precipitated under ultrasounds (NiCuUsConv and NiCuUsMwA) showed a predominant peak with a maximum around 4 nm accompanied by a peak at higher pore size (20 nm) for the sample NiCuUsMwA, probably related to the use of microwaves during aging in autoclave.

3.5.2. Basic properties

The amount of weak and strong basic sites was determined by titration with benzoic acid using bromothymol blue (pKa = 7.2) and phenolphthalein (pKa = 9.3) as indicators (Zhang et al., 2019). The results are shown in Table 4. The strong basic sites could be assigned to –OH sites present in brucite like structure while the weak basic sites correspond to carbonate species and simple metal bonded –OH group [M$(OH)_x$] present in the hydrotalcite-like materials (Navajas et al., 2010; Xi and Davis, 2008). All samples showed very low or null amount of weak basic centers. However, higher differences were observed between samples regarding the strong basic centers. In order to obtain more information, the total amount of basic centers was also calculated from

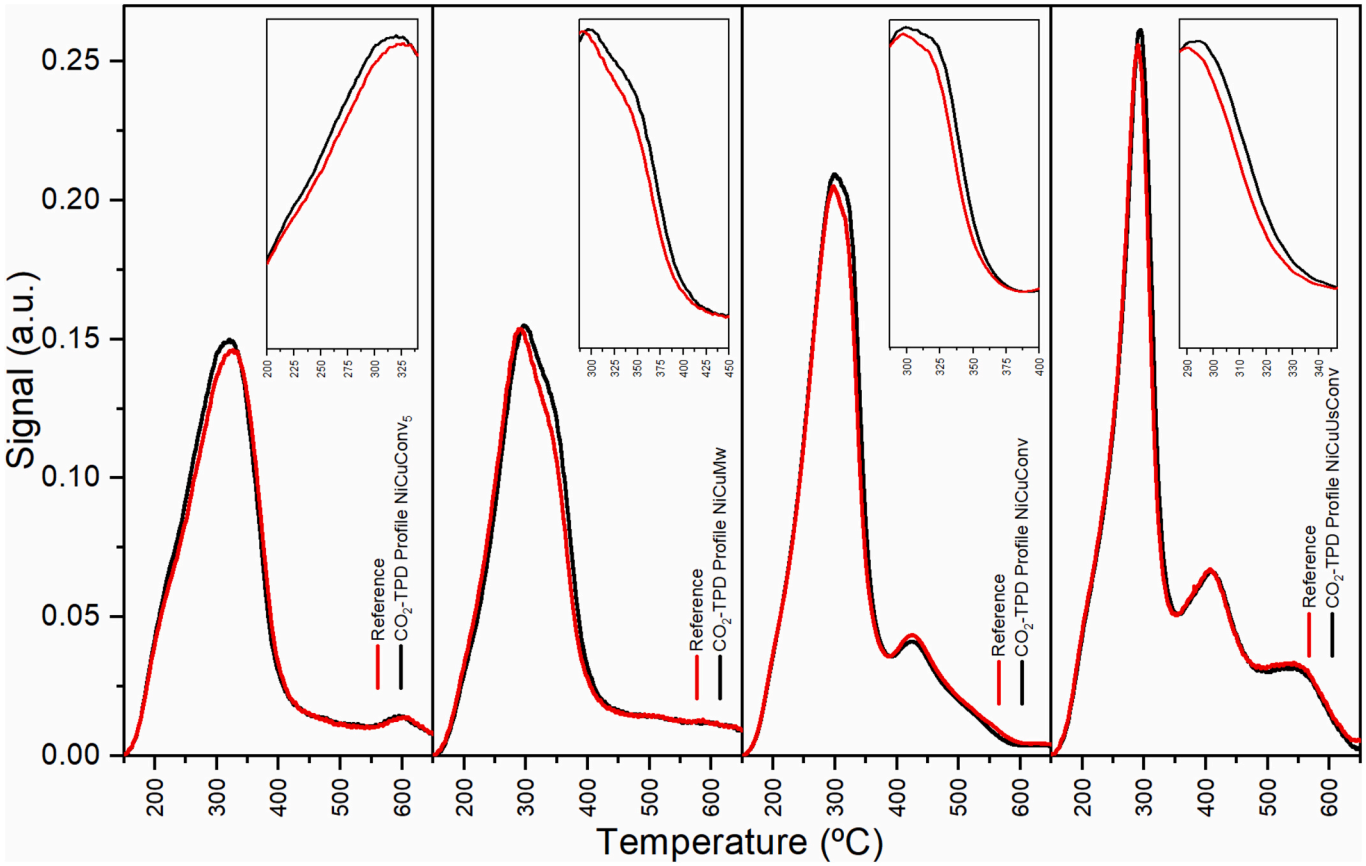

Fig. 5. CO_2-TPD of the hydrotalcite-like materials aged by refluxing.

CO_2-TPD (Table 4). The CO_2-TPDs profiles of the hydrotalcite-type materials prepared by refluxing and autoclave are shown in Fig. 5 and Fig. 6, respectively. As the layered double hydroxides decompose with temperature, a reference profile without CO_2 treatment was also recorded. Thus, the basicity of the samples was evaluated from the difference between the CO_2 desorption profile obtained after CO_2 adsorption and the decomposition profile without CO_2 treatment (reference).

The quantification of the basic sites by both methods followed the same tendency. The use of microwaves, by refluxing or autoclave, led to higher amount of basic sites. This could be related to a better incorporation of the hydroxyl groups into the layers and/or the appearance of surface-defective sites.

Furthermore, the samples precipitated with ultrasonic agitation (NiCuUsConv and NiCuUsMwA) presented lower basic values than their counterparts precipitated with magnetic agitation (NiCuConv and NiCuMwA). This could be related to the lower specific surface area of these samples (Table 4).

By comparing the thermograms, several differences between the profiles of the samples were observed (Fig. 5).

Samples $NiCuConv_5$ and NiCuMw, aged by refluxing at the same temperature and time, showed one broad peak between 200 and 400 °C with a maximum around 300 °C (Fig. 5). Interestingly, $NiCuConv_5$ had CO_2 bound to weak basic sites (desorption below 300 °C) while NiCuMw had CO_2 bound to basic sites with higher basicity strength (desorption over 300 °C). By increasing the aging time by conventional refluxing (NiCuConv), the TPD profile became more similar to that of NiCuMw (Fig. 5). As NiCuConv and NiCuMw were more crystalline than $NiCuConv_5$, this slightly stronger basicity could be related to a better availability of the hydroxyls of the layers. The use of ultrasound during precipitation (NiCuUsConv) decreased the basicity of the hydrotalcite, as observed from the less difference between the CO_2-TPD and the reference with desorption maximum at 300 °C. This could be explained by the lower crystallinity of this sample (Table 2).

For the samples aged by autoclave (Fig. 6), the use of microwaves in the sample precipitated by magnetic stirring (NiCuMwA) led to higher basicity, with CO_2 bound to basic sites at desorption temperatures in a broad range from 220 °C to 375 °C, than that aged by conventional heating at the same preparation conditions (NiCuConvA). Depending on the microwave irradiation treatment the distribution of the metals should vary generating zones more basic than others. Again, the use of ultrasound during precipitation decreased the basicity of the hydrotalcite even using microwaves for aging (NiCuUsMwA) (Fig. 6). It is important to remark that the maximum desorption temperature was higher for the autoclaved samples compared with the corresponding refluxed ones, indicating stronger basicity.

4. Conclusions

Several NiCuMgAl-LDH samples were synthesized using ultrasounds or magnetic stirring during the coprecipitation of the precursor salts, and later aging using microwaves or conventional heating and refluxing or autoclave. All samples were identified by XRD as pure hydrotalcites and their characteristic layers were observed by HRTEM for all of them. LDH materials were more crystalline when using microwaves, both by refluxing or autoclaving. This was related to the higher homogeneity of the microwaves heating. However, the use of ultrasound during coprecipitation led to less crystalline LDH. This can be explained by the formation of small crystallization nuclei due to cavitation phenomena, which delay the crystal growth during aging. By increasing the Ni^{2+}/Cu^{2+} molar ratio, the hydrotalcite crystallinity increased. Elemental analyses showed a better incorporation of the divalent cations in the layer for the samples prepared with microwaves, for the autoclaving samples and for the LDH prepared with higher Ni^{2+}/Cu^{2+} molar ratios. The TGA analyses showed higher maxima temperature values for the mass losses for the samples with higher crystallinity (prepared under microwaves and/or by autoclaving). However, the samples coprecipitated by ultrasound despite being less crystalline, had maxima temperature values for the two mass losses higher than their counterparts prepared with magnetic stirring, specially when using refluxing. This could be related to a higher stacking of the layers, as observed by HRTEM for these samples. The use of microwaves, by refluxing or autoclave, led to higher amount of stronger basic sites. This could be ascribed to a better incorporation of the hydroxyl groups into the layers and/or the appearance of surface-defective sites. In contrast, the samples coprecipitated with ultrasound had very low surface area and low amount of basic sites.

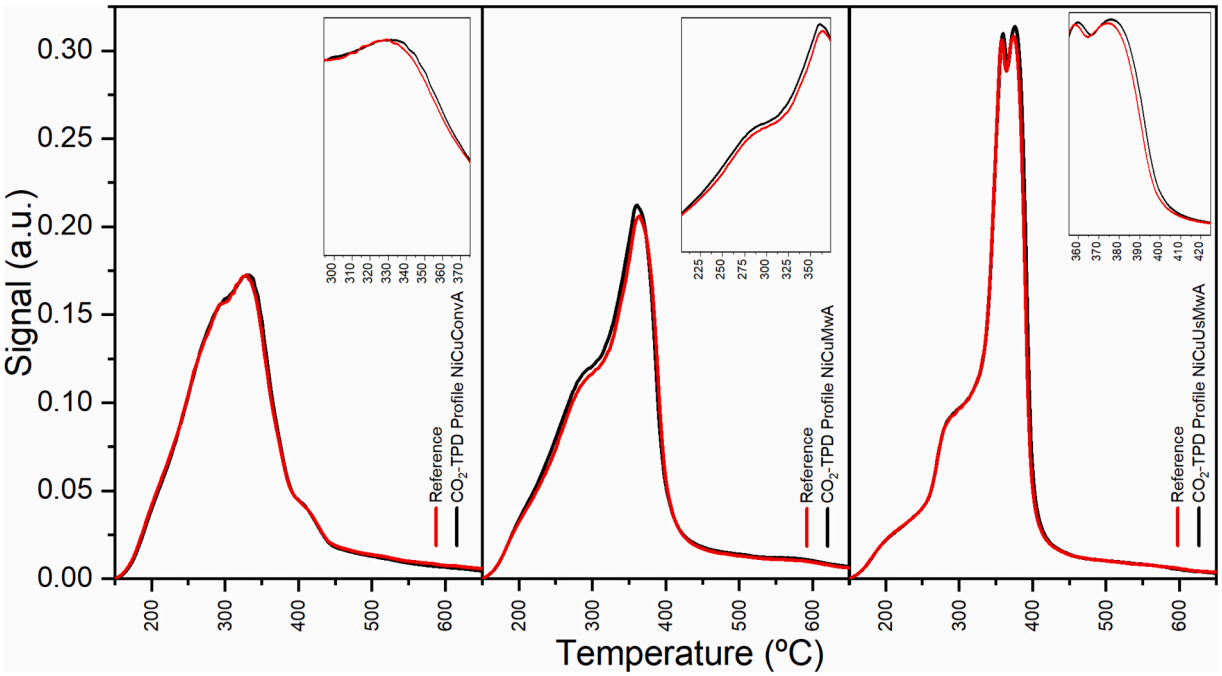

Fig. 6. CO_2-TPD of the hydrotalcite-like materials aged by autoclave.

CRediT authorship contribution statement

Judith Granados-Reyes: Writing – original draft, Visualization, Validation, Methodology, Investigation, Conceptualization. **Angie C. Rueda:** Visualization, Validation, Investigation. **Yolanda Cesteros:** Writing – review & editing, Writing – original draft, Validation, Supervision, Resources, Funding acquisition, Conceptualization.

Declaration of competing interest

The authors declare that they have no known competing financial interests or personal relationships that could have appeared to influence the work reported in this paper.

Data availability

The data that has been used is confidential.

Acknowledgments

This work was supported by the project TED2021-129487B-C31 funded by MICIU/AEI/10.13039/501100011033 and European Union NextGenerationEU/PRTR. A.C. Rueda thanks Generalitat de Catalunya for the FI grant 2022 FI_B 00128.

References

Álvarez, A., Trujillano, R., Rives, V., 2013. Differently aged gallium-containing layered double hydroxides. Appl. Clay Sci. 80–81, 326–333. https://doi.org/10.1016/j.clay.2013.05.012.

An, X., Feng, C., Ren, J., Shi, K., Du, Y., Xie, X., Wu, X., 2021. Novel highly dispersed Ni-based oxides catalysts for ethanol steam reforming. J. Energy Inst. 99, 240–247. https://doi.org/10.1016/j.joei.2021.09.015.

Ayala, A., Fetter, G., Palomares, E., Bosch, P., 2011. CuNi/Al hydrotalcites synthesized in presence of microwave irradiation. Mater. Lett. 65 (11), 1663–1665. https://doi.org/10.1016/j.matlet.2011.03.004.

Benito, P., Guinea, I., Herrero, M., Labajos, F.M., Rives, V., 2007. Incidence of microwave hydrothermal treatments on the crystallinity properties of hydrotalcite-like compounds. Z. Anorg. Allg. Chem. 633, 1815–1819. https://doi.org/10.1002/zaac.200700178.

Benito, P., Guinea, I., Labajos, F.M., Rocha, J., Rives, V., 2008. Microwave-hydrothermally aged Zn,Al hydrotalcite-like compounds: Influence of the composition and the irradiation conditions. Microporous Mesoporous Mater. 110, 292–302. https://doi.org/10.1016/j.micromeso.2007.06.013.

Bergadà, O., Vicente, I., Salagre, P., Cesteros, Y., Medina, F., Sueiras, J.E., 2007. Microwave effect during aging on the porosity and basic properties of hydrotalcites. Microporous Mesoporous Mater. 101 (3), 363–373. https://doi.org/10.1016/j.micromeso.2006.11.033.

Cavani, F., Trifirò, F., Vaccari, A., 1991. Hydrotalcite-type anionic clays: preparation, properties and applications. Catal. Today 11 (2), 173–301. https://doi.org/10.1016/0920-5861(91)80068-K.

Co-Al Ni-Al Viky-C Mujica-F, D.Y., Linares, C.F., Velásquez, I., Naguanagua Edo Carabobo Venezuela, M., 2015. The effect of treatment: Microwave radiation and co-precipitation on Co-Al and Ni-Al hydrotalcites crystal properties. Rev. LatinAm. Metal. Mat 35 (2). www.rlmm.org.

Coelho, A.A., 2018. *TOPAS* and *TOPAS-Academic* : an optimization program integrating computer algebra and crystallographic objects written in C++. J. Appl. Crystallogr. 51 (1), 210–218. https://doi.org/10.1107/S1600576718000183.

Coral, N., Brasil, H., Rodrigues, E., da Costa, C.E.F., Rumjanek, V., 2019. Microwave-modified hydrotalcites for the transesterification of soybean oil. Sustain. Chem. Pharm. 11, 49–53. https://doi.org/10.1016/j.scp.2019.01.002.

Cosano, D., Hidalgo-Carrillo, J., Esquivel, D., Romero-Salguero, F.J., Jiménez-Sanchidrián, C., Ruiz, J.R., 2020. Microwave-assisted synthesis of basic mixed oxides from hydrotalcites. J. Porous. Mater. 27 (2), 441–450. https://doi.org/10.1007/s10934-019-00825-8.

Fan, X., Li, L., Yang, X., Guo, Z., Jing, F., Chu, W., 2020. High-performance CoxM3-xAlOy (M[dbnd]Ni, Mn) catalysts derived from microwave-assisted synthesis of hydrotalcite precursors for methane catalytic combustion. Catal. Today 347, 23–30. https://doi.org/10.1016/j.cattod.2018.09.007.

Gao, G., Feng, S., Jiang, Z., Hu, C., Zhang, Q., Tsang, D.C.W., 2023. Efficient hydrogenation of glucose to polyols over hydrotalcite-derived PtNi alloy catalyst under mild conditions. Ind. Eng. Chem. Res. 62 (7), 3140–3150. https://doi.org/10.1021/acs.iecr.2c04313.

Granados-Reyes, J., Salagre, P., Cesteros, Y., 2014. Effect of microwaves, ultrasounds and interlayer anion on the hydrocalumites synthesis. Microporous Mesoporous Mater. 199, 117–124. https://doi.org/10.1016/j.micromeso.2014.08.004.

Gupta, S.S.R., Kantam, M.L., 2018. Selective hydrogenation of levulinic acid into γ-valerolactone over Cu/Ni hydrotalcite-derived catalyst. Catal. Today 309, 189–194. https://doi.org/10.1016/j.cattod.2017.08.007.

Houssaini, J., Naciri Bennani, M., Ziyat, H., Arhzaf, S., Qabaqous, O., Amhoud, A., 2021. Study of the catalytic activity of the compounds hydrotalcite type treated by microwave in the self-condensation of acetone. Intern. J. Anal. Chem. 2021. https://doi.org/10.1155/2021/1551586.

Kostić, M., Radović, M., Velinov, N., Najdanović, S., Bojić, D., Hurt, A., Bojić, A., 2018. Synthesis of mesoporous triple-metal nanosorbent from layered double hydroxide as an efficient new sorbent for removal of dye from water and wastewater. Ecotoxicol. Environ. Saf. 159, 332–341. https://doi.org/10.1016/j.ecoenv.2018.05.015.

Lee, S.C., Choi, J.H., Lee, C.W., Woo, S.H., Lee, J., Woo, H.C., 2022. H2 production by steam reforming of Saccharina japonica-derived liquefied oils on NixCuy hydrotalcite-derived catalysts. Renew. Energy 191, 418–427. https://doi.org/10.1016/j.renene.2022.03.161.

Li, J., Lin, L., Tan, Y., Wang, S., Yang, W., Chen, X., Luo, W., Ding, Y.J., 2022. High performing and Stable Cu/NiAlOx catalysts for the continuous catalytic conversion of ethanol into butanol. ChemCatChem 14 (17). https://doi.org/10.1002/cctc.202200539.

Lopes, D., Zotin, F., Palacio, L.A., 2018. Copper-nickel catalysts from hydrotalcite precursors: the performance in NO reduction by CO. Appl. Catal. B Environ. 237, 327–338. https://doi.org/10.1016/j.apcatb.2018.06.007.

Luo, L., Yuan, F., Zaera, F., Zhu, Y., 2021. Catalytic hydrogenation of furfural to furfuryl alcohol on hydrotalcite-derived CuxNi3−xAlOy mixed-metal oxides. J. Catal. 404, 420–429. https://doi.org/10.1016/j.jcat.2021.10.009.

Naseem, S., Gevers, B., Boldt, R., Labuschagné, F.J.W.J., Leuteritz, A., 2019. Comparison of transition metal (Fe, Co, Ni, Cu, and Zn) containing tri-metal layered double hydroxides (LDHs) prepared by urea hydrolysis. RSC Adv. 9 (6), 3030–3040. https://doi.org/10.1039/c8ra10165e.

Navajas, A., Campo, I., Arzamendi, G., Hernández, W.Y., Bobadilla, L.F., Centeno, M.A., Odriozola, J.A., Gandía, L.M., 2010. Synthesis of biodiesel from the methanolysis of sunflower oil using PURAL® Mg-Al hydrotalcites as catalyst precursors. Appl. Catal. B Environ. 100 (1–2), 299–309. https://doi.org/10.1016/j.apcatb.2010.08.006.

Niu, J., Ma, Z., Zhang, Y., Shi, J., Yang, L., Yao, B., Yu, X., Wei, H., 2022. Optimization of microwave process parameters in preparation of ni-fe hydrotalcite by response surface methodology and evaluation of photocatalytic degradation of antibiotic wastewater. Integr. Ferroelectr. 228 (1), 192–201. https://doi.org/10.1080/10584587.2022.2072134.

Stokes, A.R., Wilson, A.J.C., 1942. A method of calculating the integral breadths of Debye-Scherrer lines. Math. Proc. Camb. Philos. Soc. 38 (3), 313–322. https://doi.org/10.1017/S0305004100021988.

Summa, P., Samojeden, B., Motak, M., Wierzbicki, D., Alxneit, I., Świerczek, K., Da Costa, P., 2022. Investigation of Cu promotion effect on hydrotalcite-based nickel catalyst for CO2 methanation. Catal. Today 384–386, 133–145. https://doi.org/10.1016/j.cattod.2021.05.004.

Trujillano, R., González-García, I., Morato, A., Rives, V., 2018. Controlling the synthesis conditions for tuning the properties of hydrotalcite-like materials at the nano scale. ChemEngineering 2 (3), 1–15. https://doi.org/10.3390/chemengineering2030031.

Wang, J., Zhang, T., Li, K., Cao, Y., Zeng, Y., 2018. Dehydrogenation catalysts for synthesis of O-phenylphenol via Cu/Ni/Mg/Al hydrotalcite-like compounds as precursors. Catalysts 8 (5). https://doi.org/10.3390/catal8050186.

Wang, L., Li, B., Chen, C., Jia, L., 2010. Structural characterization and related properties of the stearate anions intercalated Ni-Al hydrotalcite-like compound prepared by the microwave crystallization. J. Alloys Compd. 508 (2), 426–432. https://doi.org/10.1016/j.jallcom.2010.08.080.

Wang, Z., Yin, M., Pang, J., Li, X., Xing, Y., Su, Y., Liu, S., Liu, X., Wu, P., Zheng, M., Zhang, T., 2022. Active and stable Cu doped NiMgAlO catalysts for upgrading ethanol to n-butanol. J. Energy Chem. 72, 306–317. https://doi.org/10.1016/j.jechem.2022.04.049.

Wei, Y., Ni, W., Zhang, C., You, K., Zhao, F., Chen, Z., Ai, Q., Luo, H., 2022. Highly Dispersed and Stable Hydrotalcite-Derived NiCu/MgAlO Alloy Catalyst for Efficient Amination of Cyclohexanol to Cyclohexylamine in the Vapor phase. ACS Sustain. Chem. Eng. 10 (40), 13367–13379. https://doi.org/10.1021/acssuschemeng.2c03505.

Wei, Y., You, K., Xu, W., Ou, X., Zhao, F., Chen, Z., Yan, D., Zhang, X., Luo, H., 2023. Highly efficient reductive amination of ethanol to ethylamines over non-noble metallic NiCu/MgAlO catalyst. Ind. Eng. Chem. Res. 62 (12), 4947–4954. https://doi.org/10.1021/acs.iecr.3c00083.

Wu, J., Gao, G., Li, J., Sun, P., Long, X., Li, F., 2017. Efficient and versatile CuNi alloy nanocatalysts for the highly selective hydrogenation of furfural. Appl. Catal. B Environ. 203, 227–236. https://doi.org/10.1016/j.apcatb.2016.10.038.

Xi, Y., Davis, R.J., 2008. Influence of water on the activity and stability of activated Mg{single bond}Al hydrotalcites for the transesterification of tributyrin with methanol. J. Catal. 254 (2), 190–197. https://doi.org/10.1016/j.jcat.2007.12.008.

Yu, X., Zhang, F., Chu, W., 2016. Effect of a second metal (Co, Cu, Mn or Zr) on nickel catalysts derived from hydrotalcites for the carbon dioxide reforming of methane. RSC Adv. 6 (74), 70537–70546. https://doi.org/10.1039/c6ra12335j.

Zhang, J., Li, X., Xu, M., Yang, Y., Li, Y., Liu, N., Meng, X., Chen, L., Shi, S., Wei, M., 2019. Glycerol aerobic oxidation to glyceric acid over Pt/hydrotalcite catalysts at room temperature. Sci. Bull. 64 (23), 1764–1772. https://doi.org/10.1016/j.scib.2019.10.003.